Available online at www.sciencedirect.com
ScienceDirect
Journal of Power Sources 171 (2007) 363–372
JOURNAL OF POWER SOURCES
www.elsevier.com/locate/jpowsour

Effect of morphological properties of ionic liquid-templated mesoporous anatase TiO_2 on performance of PEMFC with Nafion/TiO_2 composite membrane at elevated temperature and low relative humidity

S.Y. Chen, C.C. Han, C.H. Tsai, J. Huang, Y.W. Chen-Yang *

Department of Chemistry and Center for Nanotechnology, Chung Yuan Christian University, Chung-Li 32023, Taiwan, ROC

Received 24 April 2007; received in revised form 24 May 2007; accepted 4 June 2007
Available online 23 June 2007

Abstract

Three high-purity TiO_2 (anatase) powders (T_{PF6}, T_{BF4}, and $T_{conventional}$) were prepared by the sol–gel method with/without ionic liquid as template and calcinations at 450 °C. These powders were, then, characterized to investigate their differences in morphological properties. Electrochemical performances of the H_2/O_2 PEMFCs employing the Nafion composite membranes with these three TiO_2 powders as fillers were studied over 80–120 °C under 50% and 95% relative humidity (RH). The result showed that the order of the fillers effect on the performance at 80 and 90 °C was the same as that of the TiO_2 filler's specific surface area (i.e. $T_{PF6} > T_{conventional} > T_{BF4} >$ P25, a commercially available nonporous TiO_2 powder). However, the order between $T_{conventional}$ and T_{BF4} was reversed at 110 and 120 °C under 50% RH. This indicates that the size and the amount of mesopores, which better confined the water molecules, were significant contributing factors to the performances at the higher temperatures. The best power density obtained under 50% RH at 120 °C and a voltage of 0.4 V was from the PEMFC with the T_{PF6}-containing Nafion composite membrane. It was about 5.7 times higher than the value obtained from that with the recast Nafion membrane.

Keywords: Mesoporous anatase TiO_2; Nafion/TiO_2 composite membrane; PEMFC; Ionic liquid; Morphological properties; Cell performance

1. Introduction

Proton exchange membrane fuel cells (PEMFCs) have attracted worldwide attention since they are clean energy sources for electric vehicles and residences. Dupont's Nafion® is one of the most common commercially available perfluorinated ionomer membranes used today [1]. However, water loss from the proton exchange membrane leads to a drastic drop in proton conductivity with a consequent decrease in the overall fuel cell efficiency [2–6]. This disadvantage has limited the operation temperature of PEMFC under 100 °C. To solve this problem, considerable efforts have been focused on the development of membrane materials capable of maintaining proper hydration by the addition of nanocrystalline ceramic oxides [2–22]. The results showed that the modification of the polymer host membrane by the incorporation of hygroscopic ceramic oxides, such as ZrO_2, SiO_2, and TiO_2 particles, into Nafion has effectively extended the working temperature range. The improvement was attributed to the presence of the filler which was beneficial in maintaining the hydration of the membrane and improving the mechanical properties, as well as for increasing the degree of tortuosity of the methanol crossover pathway [23,24] as used in direct methanol fuel cell (DMFC).

Studies on Nafion/TiO_2 composite membranes have also attracted the attention of many research groups which showed that the effect of the morphological properties of the filler plays a key role in determining the water retention properties of the composite membranes at a high operating temperature [2,3,6,7,21,22]. In addition, they showed that such effect is more important than the crystalline structure of the filler [2]. However, a detailed study of the effect of the morphological properties of mesoporous TiO_2 filler on PEMFC performance, especially at high temperature and low relative humidity, has not been reported.

As is known, metal oxide materials are mainly prepared by the sol–gel method, and the morphological properties of

* Corresponding author. Tel.: +886 3 265 3317; fax: +886 3 265 3399.
E-mail address: yuiwhei@cycu.edu.tw (Y.W. Chen-Yang).

0378-7753/$ – see front matter © 2007 Elsevier B.V. All rights reserved.
doi:10.1016/j.jpowsour.2007.06.047

the oxides are primarily determined by the synthetic conditions applied, especially the template used [25,26]. In general, ionic or nonionic surfactants are used as the template [27–30]. Recently, a water-immiscible room-temperature ionic liquid (RTIL), [Bmim][PF_6], was used as an effective templating material in the modified sol–gel procedure to prepare the nanocrystalline TiO_2 particles [31]. The TiO_2 particles not only exhibited good morphological properties, including high surface area, stable crystal structure, controlled porosity, and tailor-designed pore size distribution, but also showed good thermal stability and kept a highly porous structure even after calcinations.

The aim of this study is to better understand how Nafion-based composite membranes containing mesoporous TiO_2 fillers with different morphological properties influence the performance of PEMFC. Three different porous TiO_2 powders, T_{PF6}, T_{BF4}, and $T_{conventional}$, were prepared by the modified sol–gel method mentioned above either with [Bmim][PF_6], [Bmim][BF_4], or without ionic liquid template, followed by calcination at 450 °C. The corresponding Nafion/TiO_2 composite membranes were then prepared from 3 and 10 wt.% of these porous TiO_2 powders to perform their respective H_2/O_2 PEMFC cell tests. In addition, the cell test results of these PEMFCs were compared to the PEMFC with the recast Nafion membrane and the membrane incorporated with a commercially available nonporous TiO_2.

2. Experimental

2.1. Chemicals and materials

A room-temperature ionic liquid, 1-butyl-3-methylimidazolium tetrafluoroborate [Bmim][BF_4], was prepared by the metathesis of 1-butyl-3-methylimidazolium chloride and sodium tetrafluoroborate ($NaBF_4$, 98%, Acros) as reported [32]. The commercially available 5 wt.% Nafion solution (DuPont, equivalent weight = 1100 g mol^{-1} SO_3H) and the ionic liquid 1-butyl-3-methylimidazolium hexafluorophosphate, [Bmim][PF_6] (Merck) were used as received. Other chemicals including TiO_2 powder (P25, Degussa), 1-methylimidazole (99%, Acros), sodium tetrafluoroborate (98%, Acros), titanium tetraisopropoxide (TTIP, 98%, Acros), isopropyl alcohol (i-PrOH, Aldrich), acetone (Aldrich), acetonitrile (Aldrich), *N*,*N*-dimethylacetamide (DMAc, 99.5%, Tedia), hydrogen peroxide (H_2O_2, 30–35%, Showa), and sulfuric acid (H_2SO_4, 97%, Showa) were of reagent grade and were used without further purification.

2.2. Preparation of the anatase TiO_2 powders

The mesoporous anatase TiO_2 powders were prepared by a modified procedure [31]. A typical example is described as follows: titanium tetraisopropoxide was mixed with isopropanol at the i-PrOH/TTIP molar ratio of 30. The ionic liquid, 1-butyl-3-methylimidazolium hexafluorophosphate ([Bmim][PF_6]), was then added into the mixed solution at the [Bmim][PF_6]/TTIP molar ratio of 3 and then stirred for 10 min. Afterwards, the mixed solution was added dropwise into the deionized water up to a H_2O/TTIP molar ratio of 100 at room temperature. The solution was stirred vigorously for 30 min, and the TiO_2 particles were recovered by filtration, washed thoroughly with deionized water, and dried in a freeze-dryer (Eyela FDU-1200, Tokyo Rikakikai) under 15 Pa at −50 °C for 12 h. The entrapped [Bmim][PF_6] and organics were extracted by refluxing with acetonitrile for 12 h. The TiO_2 particles were recovered again by filtration, washed with deionized water, and dried in a freeze-dryer. The final product was a white powder. For comparison, a relatively water-miscible room-temperature ionic liquid, 1-butyl-3-methylimidazolium tetrafluoroborate ([Bmim][BF_4]), was also used as a template, instead of [Bmim][PF_6], to prepare the TiO_2 particles by the same preparative procedure. In order to obtain high-purity TiO_2 powders, the products were further heated to 450 °C with a heating rate of 1 °C min^{-1} and calcined at 450 °C for 3 h after the extraction process. For an additional comparison, another anatase TiO_2 was prepared by the same process without using the template. For convenience, the abbreviations T_{PF6}, T_{BF4}, and $T_{conventional}$ were used to denote the TiO_2 particles prepared with [Bmim][PF_6], [Bmim][BF_4], and without ionic liquid, respectively.

2.3. Characterization of the TiO_2 powders and Nafion/TiO_2 composite membranes

The thermogravimetric analysis of the powders was conducted from 30 to 550 °C under air flow of 60 mL min^{-1} with a Seiko TG/DTA-220 thermal analyzer at a heating rate of 2 °C min^{-1}.

A wide-angle powder X-ray diffraction (XRD) study of the crystal phase of the TiO_2 powders was performed on a Rigaku D/MAX-3COD-2988N X-ray diffractometer with a copper target ($\lambda = 0.154$ nm) and a nickel filter at a scanning rate of 2° min^{-1}. For each scan, 2θ was increased from 20.0° to 60.0° with a step of 0.1° and a time-to-step ratio of 1.0.

Particle size of the as-prepared TiO_2 powder was measured using a particle size analyzer (Brookhaven 90Plus). Before measurement, the TiO_2 powder was dispersed in a 1.0 mM NaCl solution by stirring vigorously and vibrating homogeneously in an ultrasonator (Sonics, VCX-750) for 30 min.

The pore volume, pore size distribution, and Brunauer–Emmett–Teller (BET) surface area of the TiO_2 powders were determined by a Micromeritics ASAP2010 analyzer at 77 K. The samples were purged with helium gas at 120 °C for 3 h prior to the measurements of nitrogen adsorption and desorption isotherms.

The morphologies of the TiO_2 powders were measured using JEOL TEM-2010 transmission electron microscopy (TEM) at 200 kV. The samples were embedded in Spurr's epoxy resin, microtomed to 80 nm thickness, and mounted on 3 mm TEM grids for examination.

Fourier transform infrared (FT-IR) spectra of the synthesized TiO_2 powders were recorded on a Bio-Rad FTS-7 spectromer with a wavenumber resolution of 2 cm^{-1} in the range of 400–4000 cm^{-1} as KBr pellets at a ratio of sample:KBr = 1:100.

The morphologies of the composite membranes were investigated by scanning electron microscopy (SEM) using LV-3500N (for surface) and S-3000N (for cross-section) of Hitachi instruments. Before measurements, the samples were coated with a layer of gold to enhance electrical conduction.

The dehydration rates of the membranes were measured as follows: the membranes were boiled in deionized water at 100 °C for 1 h, taken out and wiped off the surface moisture with absorbed paper, and weighed (W_1). Then the membranes were put in an oven at the selected temperature and 50% RH for 30 min, and weighed (W_2). The dehydration rate of the sample is defined by the following equation:

$$\text{dehydration rate (\%/min)} = \left(\frac{((W_1 - W_2)/W_1) \times 100}{30} \right)$$

2.4. Preparation of the composite membranes and membrane electrode assembly

All the Nafion/TiO_2 composite membranes were prepared using the recast procedure. The original 5 wt.% DuPont Nafion solution was evaporated under vacuum at 60 °C until a dry residue was obtained. The residual Nafion resin was redissolved in a desired amount of DMAc to form a solution containing 5 wt.% of Nafion. An appropriate amount of TiO_2 powder was added and dispersed in an ultrasonic bath. The resulting mixture was cast onto a stainless steel cell and was slowly evaporated at 80 °C to remove most of the solvent. The membrane was heated to 160 °C and allowed to dry completely. The membrane was cooled, and was further purified by successive chemical treatments with 5% H_2O_2, 1N H_2SO_4, and deionized water. A membrane of thickness around 80 μm was obtained from 3 or 10 wt.% TiO_2 loading. A recast Nafion membrane was also prepared with the same procedure for comparative study.

2.5. The PEMFC test for the Nafion-based membranes

Fuel cell efficiency tests were performed on the membrane electrode assemblies (MEAs) prepared with the recast Nafion membrane and the as-prepared Nafion/TiO_2 composite membranes. The gas diffusion layer used in the MEAs was a carbon cloth (E-TEK) pretreated with FEP resin (DuPont) and carbon powder (XC-72, Carbot). The catalyst inks were prepared by mixing catalyst powder (20 wt.% Pt/C, E-TEK), 5 wt.% Nafion solution, and isopropyl alcohol. The Pt/C catalyst content of anode was 0.2 mg cm^{-2} and that of cathode was 0.4 mg cm^{-2}. The MEA was assembled using a hot pressing process. Two electrodes with an effective area of 5 cm^2 were hot-pressed to one piece of membrane at 140 °C and 70–90 kg cm^{-2} for 2–3 min to make a sandwich-type MEA, and then the MEA was positioned in a single cell which was installed in a fuel cell test system. The single cell was operated under the cell temperature: 80–120 °C; gas purity: 99.9% for H_2 and 99.0% for O_2. The RH (50% and 95%) was controlled by controlling the water temperature of the H_2 and O_2 gas humidification bottle. The anode H_2 input flow rate was 540 mL min^{-1}, and the cathode O_2 input flow rate was 360 mL min^{-1}.

Table 1
Abbreviations and compositions of the Nafion-based membranes

Abbreviation of the composite membrane	The composition of the composite membrane	The abbreviation of the corresponding PEMFCs
RNF	Recast Nafion	PEM-RNF
NF3P	Nafion/3 wt.% T_{PF6}	PEM-NF3P
NF3B	Nafion/3 wt.% T_{BF4}	PEM-NF3B
NF3C	Nafion/3 wt.% $T_{conventional}$	PEM-NF3C
NF3N	Nafion/3 wt.% P25	PEM-NF3N
NF10P	Nafion/10 wt.% T_{PF6}	PEM-NF10P
NF10B	Nafion/10 wt.% T_{BF4}	PEM-NF10B
NF10C	Nafion/10 wt.% $T_{conventional}$	PEM-NF10C
NF10N	Nafion/10 wt.% P25	PEM-NF10N

The abbreviations and the composition of the membranes and the corresponding PEMFCs prepared are summarized in Table 1.

3. Results and discussion

3.1. Characterization of the TiO_2 particles

Fig. 1 shows the FT-IR spectra of T_{PF6} before and after extraction by acetonitrile. By comparison, the difference between the two spectra, especially the disappearance of the characteristic absorbance of the [Bmim][PF_6] at around 2900 cm^{-1} and 1250–1550 cm^{-1}, reveals that most of the entrapped [Bmim][PF_6] was removed from the TiO_2 particles by the extraction process. Nevertheless, as shown in Fig. 2, the TGA thermograms show that the weight loss of the solvent-extracted TiO_2 samples was about 21% (±2%) below 450 °C, indicating that other than the adsorbed and condensed water, few organic residues remained in the TiO_2 network. Since no significant weight change is found above 450 °C in all the thermograms, the samples were further calcined at 450 °C after the extraction process to obtain high-purity TiO_2 powders.

The averaged particle size of the as-synthesized T_{PF6}, T_{BF4}, and $T_{conventional}$ measured by the particle-size analyzer was 95,

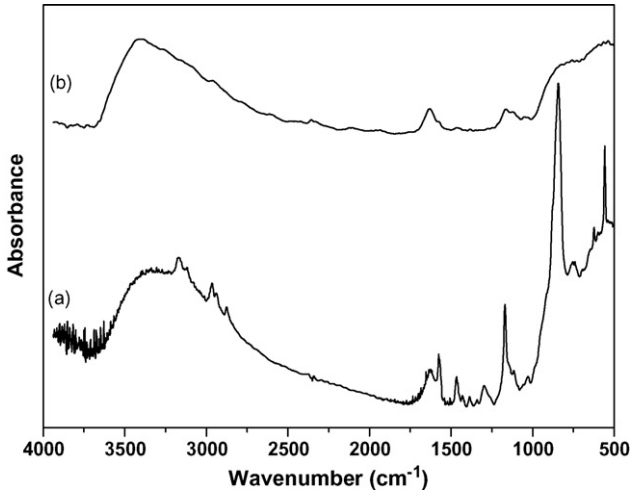

Fig. 1. FT-IR spectra of the T_{PF6} sample (a) before and (b) after the solvent extraction.

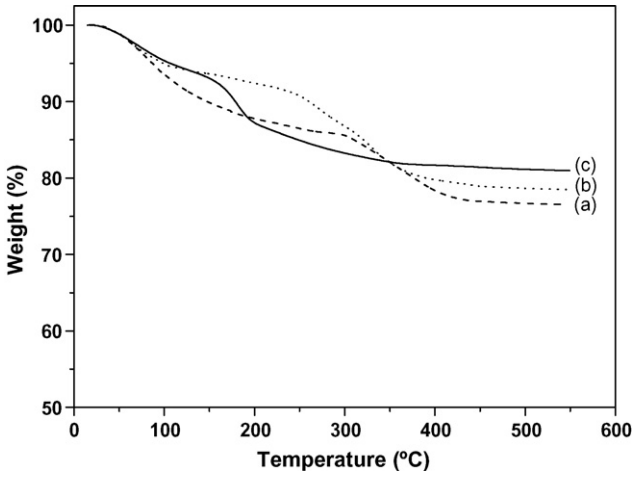

Fig. 2. TGA curves of the TiO_2 samples after solvent extraction: (a) T_{PF6}, (b) T_{BF4}, and (c) $T_{conventional}$.

182 and 215 nm, respectively. This indicates that T_{PF6} and T_{BF4}, the ionic liquid-templated TiO_2 powders, were less aggregated than $T_{conventional}$. After calcination, the particle sizes of all the powders were increased significantly, as expected. Nevertheless, the order of their averaged particle sizes remained the same, i.e. T_{PF6} (317 nm) < T_{BF4} (454 nm) < $T_{conventional}$ (607 nm), revealing that the order in the degree of aggregation due to the heat treatment did not change as well. The result suggests that T_{PF6} and T_{BF4} would have larger specific surface area than $T_{conventional}$, and T_{PF6} would posses the largest among them.

The FT-IR spectra of the calcined TiO_2 powders show characteristic absorbance between 500 and 900 cm^{-1} for the oxide structure as shown in Fig. 3. The broad band around 3400 cm^{-1} and the peak at 1650 cm^{-1} are observed due to the surface adsorbed water [33]. The fact that no absorption is seen between 1000 and 1600 cm^{-1} (the main characteristic absorbance region for the ionic liquids and the organic species) confirms the high purity of the as-prepared TiO_2 powders.

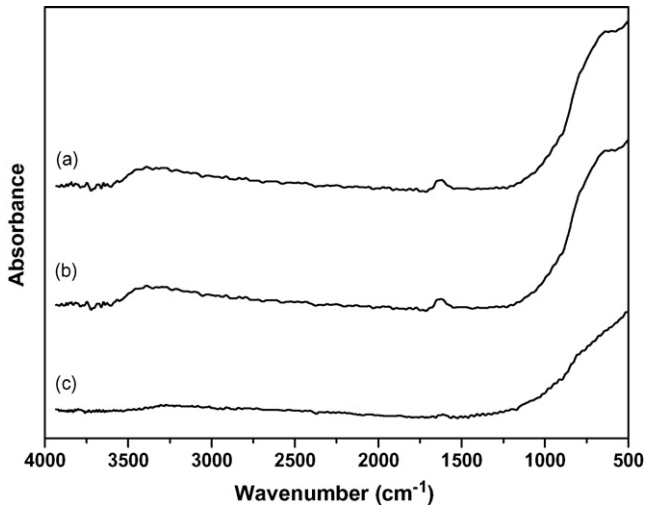

Fig. 3. FT-IR spectra of the 450 °C-calcined TiO_2 samples: (a) T_{PF6}, (b) T_{BF4}, and (c) $T_{conventional}$.

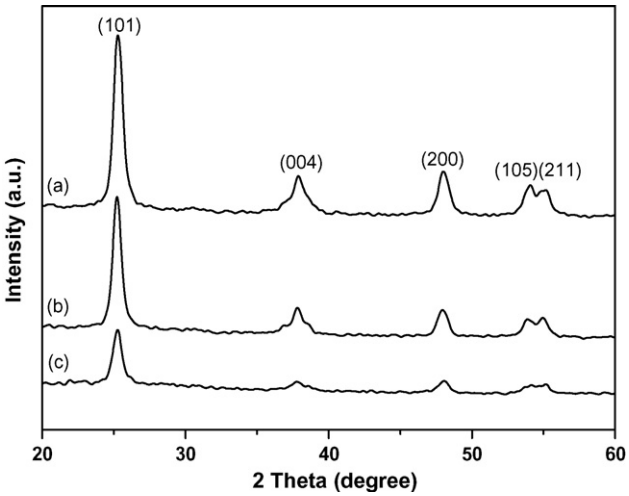

Fig. 4. XRD patterns of the 450 °C-calcined TiO_2 samples: (a) T_{PF6}, (b) T_{BF4}, and (c) $T_{conventional}$.

Fig. 4 presents the X-ray diffraction patterns of the three calcined TiO_2 samples. It indicates that all the calcined samples possess the crystallographic structure of anatase. From the broadness of the (1 0 1) peaks, the crystallite sizes in the three samples were calculated to be 10.7, 11.7, and 12.1 nm, for T_{PF6}, T_{BF4}, and $T_{conventional}$, respectively, using Scherrer's equation [34].

For comparison, the TEM images of the TiO_2 particles calcined at 150 °C are shown with that at 450 °C in Fig. 5. As can be seen, a similar wormhole-like mesoporous framework with a different pore size is observed in each of the three images of the 150 °C-calcined samples. On the other hand, the images of the 450 °C-calcined samples show that the framework of T_{PF6} was kept better than that of T_{BF4}, indicating that the network structure of T_{PF6} is more stable than that of T_{BF4} under the calcination. As for $T_{conventional}$, it is found that the morphology was obviously rearranged, and the pores were changed to larger sizes accordingly. This means that the initial inorganic network had been collapsed, and the aggregation of the TiO_2 particles occurred after the high temperature treatment. This reveals that the network structure of $T_{conventional}$ is quite unstable under the 450 °C calcination. Above all, the results indicate that the network structure of the TiO_2 particles prepared with the ionic liquids showed better thermal stability than that prepared without using ionic liquid, and that the thermal stability of the network structure is also varied with the type of anion of the ionic liquid. This may be attributed to the stronger hydrogen bonding between the water molecules and the $[BF_4]^-$ anions than that between water and the $[PF_6]^-$ anions [31].

Fig. 6 shows the adsorption–desorption isotherms of T_{PF6}, T_{BF4}, and $T_{conventional}$. It indicates that the isotherms of T_{PF6} and T_{BF4} are type IV based on the Brunauer, Deming, Deming, and Teller (BDDT) classification [35], confirming that both the ionic liquid-templated TiO_2 samples, T_{PF6} and T_{BF4}, are typical mesoporous materials. The gas adsorption occurs in the micropores at a very low pressure. It is then followed by adsorption in the mesopores, with capillary condensation occurring at the higher pressures, which leads to the broad hysteresis loops [36].

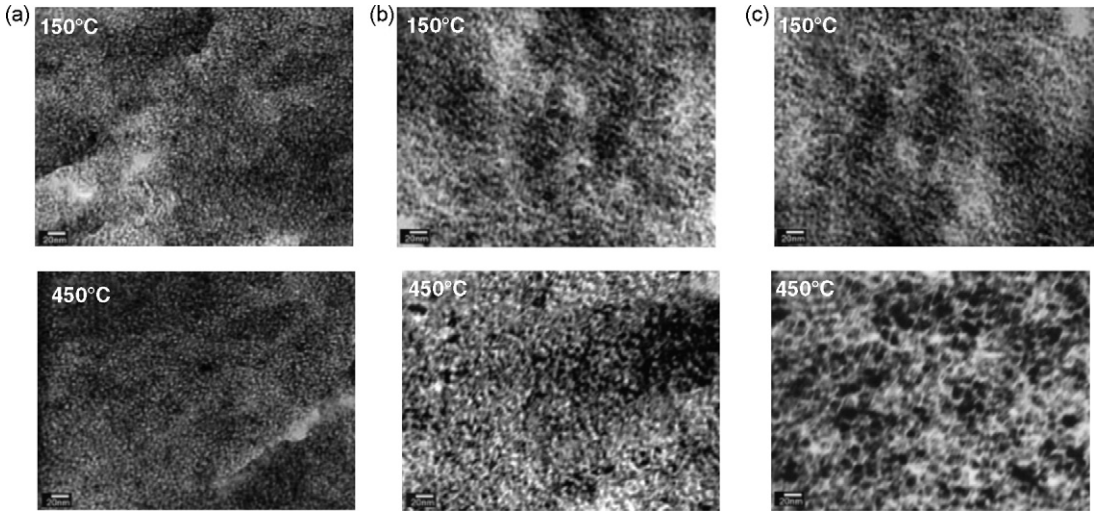

Fig. 5. TEM images of the TiO_2 samples calcined at 150 and 450 °C: (a) T_{PF6}, (b) T_{BF4}, and (c) $T_{conventional}$.

On the other hand, the isotherm of $T_{conventional}$, the TiO_2 prepared without ionic liquid, shows a type I curve with instant rise in adsorbed quantity at a low pressure, which rapidly reaches saturation as pressure increased, indicating that the majority of the pores in $T_{conventional}$ are micropores [37]. The small hysteresis loop of the desorption isotherm observed in the middle pressure range reveals that only a very small amount of mesoporous pores is present in the $T_{conventional}$ powder. This is consistent with the result obtained from the TEM micrographs. The parameters measured from the isotherms, characterizing the morphological features of the three synthesized TiO_2, are summarized with that of P25 in Table 2. The Brunauer–Emmett–Teller (BET) specific surface area (SSA) of the 450 °C-calcined T_{PF6}, T_{BF4}, and $T_{conventional}$ samples are 122, 82, and 89 $m^2\,g^{-1}$, respectively. Obviously, all the as-prepared TiO_2 have higher SSA than the nonporous P25 (SSA = 46 $m^2\,g^{-1}$) as expected for the porous materials. However, the SSA of T_{PF6} is significantly higher than that of the other two, confirming that the morphological structure of T_{PF6} was better retained than T_{BF4} and $T_{conventional}$ under the calcinations as discussed above. Furthermore, the insets of Fig. 6(a and b) show a narrow Barret–Joyner–Halenda (BJH) mesopore distribution ranging from 6 to 13 nm maximum centered at 8.3 nm and 10–16 nm maximum centered at around 14.5 nm for T_{PF6} and T_{BF4}, respectively. The measured values of the corresponding BJH pore diameter based on the adsorption isotherm are 8.3 and 14.3 nm for T_{PF6} and T_{BF4}, respectively, which are quite similar to those based on desorption isotherm, 8.0 and 13.9 nm. This implies that the mesopores in T_{BF4} are larger than those in T_{PF6}, and both mesoporous structures remained quite homogeneous after the calcinations as shown in the TEM micrographs. As shown in the inset of Fig. 6(c) the BJH mesopore distribution is broader in $T_{conventional}$ by between 5 and 18 nm. This indicates not only that the quantity of the mesopores in $T_{conventional}$ is small but also the pore-sizes of this small amount of mesopores are distributed in a larger range. This also supports the change in pore structure under calcinations. In addition, the specific pore volumes obtained are 0.25 and 0.40 $cm^3\,g^{-1}$ for T_{PF6} and T_{BF4}, respectively, revealing that the porosity of the calcined TiO_2 samples is also varied due to the different morphologies formed during the preparation process. No specific pore volume of $T_{conventional}$ is indicated in this table because its largest contribution comes from the larger pores formed after calcination as shown in the TEM micrograph.

3.2. The properties and the performance of the Nafion/TiO_2 composite membranes

In order to investigate the effect of the morphological properties in each of the as-prepared mesoporous TiO_2 fillers on the performance of the corresponding Nafion-based composite membrane in PEMFC at a high temperature and low RH, a series of Nafion/TiO_2 composite membranes containing the different TiO_2 fillers with 3 and 10 wt.% loading was fabricated.

Table 2
Morphological parameters of the TiO_2 particles prepared under different synthetic conditions

TiO_2	Synthetic condition	Temperature (°C)	Crystal phase	SSA_{BET} ($m^2\,g^{-1}$)[a]	V_{pore} ($cm^3\,g^{-1}$)[a]	D_{BJH} (nm)[a]	CS_{XRD} (nm)[b]
T_{PF6}	[Bmim][PF_6]	450	Anatase	122	0.25	8.3	10.7
T_{BF4}	[Bmim][BF_4]	450	Anatase	82	0.40	14.3	11.7
$T_{conventional}$	Without ionic liquid	450	Anatase	89	–	12.5	12.1
P25	–		A:R = 3:1[c]	46	–	–	–

[a] V_{pore}, pore volume; SSA_{BET}, BET surface area; D_{BJH}, BJH average pore diameter from N_2 adsorption isotherm branch.
[b] Crystallite size measured from XRD with Scherrer's equation.
[c] A:R indicates the ratio of anatase and rutile crystal phases provided by Degussa.

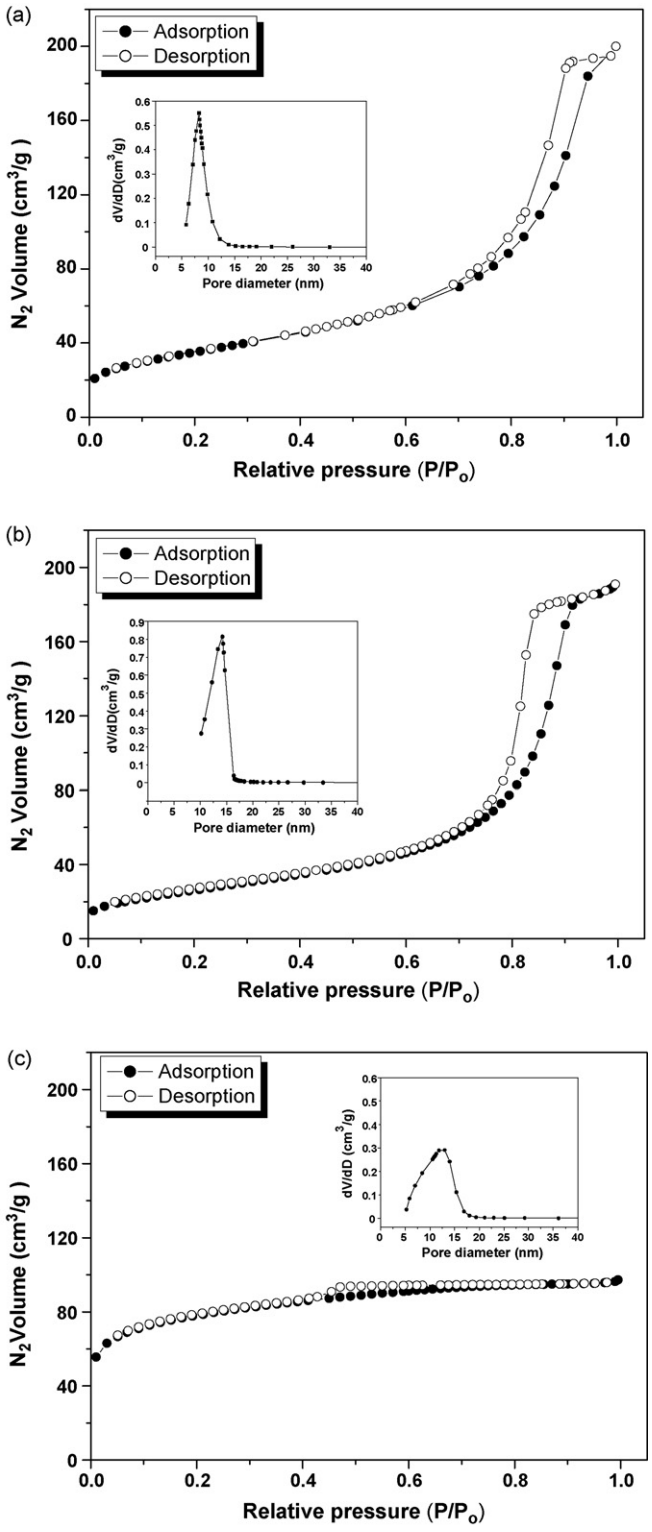

Fig. 6. Nitrogen adsorption–desorption isotherms and pore size distribution (inserted) of the TiO_2 samples: (a) T_{PF6}, (b) T_{BF4}, and (c) $T_{conventional}$.

It was found that all the as-prepared composite membranes appeared translucent and no separated filler-phase was observed in the bottom of the membrane, implying that the TiO_2 powders were homogeneously dispersed in the Nafion matrix. The typical SEM microphotographs and the corresponding SEM-EDS Ti mappings for the surface and cross-section of NF3P are shown in Fig. 7 as an example of the as-prepared Nafion/TiO_2 composite membranes. As can be seen, the mesoporous TiO_2 powders are well distributed in the Nafion matrix. This confirms that the fillers did not aggregate to form a separate phase and the composite membranes all appeared as single-layer membranes.

The cell tests of the as-fabricated H_2/O_2 PEMFCs were carried out at different temperatures and relative humidity, and the efficiencies were evaluated based on their cell voltage versus current density (polarization) curves.

Fig. 8 shows the polarization and power density curves recorded at 80 °C and 95% RH for the various PEMFCs equipped with the recast Nafion and the as-prepared Nafion/TiO_2 composite membranes. The current density delivered at a cell voltage of 0.4 V and the corresponding power density for NF3P, NF3C, NF3B, NF3N, and recast Nafion (RNF) are 2254, 1803, 1625, 1379, and 1520 mA cm^{-2}, and 893, 714, 644, 546, and 602 mW cm^{-2}, respectively. Thus, the values for the composite membranes containing T_{PF6}, $T_{conventional}$, T_{BF4}, and P25 are 1.48, 1.19, 1.07, and 0.91 times of that containing RNF. That is, the decreasing order of the enhancement of the filler on the current density of the PEMFC is $T_{PF6} > T_{conventional} > T_{BF4} > P25$. This indicates that other than the composite membrane (NF3N) with the nonporous TiO_2 filler, P25, all the composite membranes delivered a higher current density than the recast unmodified Nafion membrane.

The lower current density of the one with P25 has the following explanation. At the condition of a high RH of 95% and a relatively low temperature of 80 °C, the recast membrane contained sufficient moisture to assist the conduction of the protons. Although P25 is hygroscopic with water adsorption capability, the interfaces between the Nafion matrix and the P25 particles could possibly interfere with the proton transport a little bit, such that the advantage of the water retention capability of the nonporous P25 particles is not sufficient to overcome the reduction of proton conduction. However, as the temperature was raised to above 90 °C, the efficiency of PEM-NF3N became higher than that of PEM-RNF. This is attributed to that of water retention ability which becomes a more important factor at this temperature. A similar trend is observed in the performance of the composite membranes containing 10 wt.% of the as-prepared TiO_2 fillers. It is also noticed that the order is consistent with the order of their SSA values, i.e. T_{PF6} (122 m^2 g^{-1}) > $T_{conventional}$ (89 m^2 g^{-1}) > T_{BF4} (82 m^2 g^{-1}) > P25 (46 m^2 g^{-1}), indicating that the higher the surface area of the filler, the higher the performance efficiency of the corresponding PEMFC with both 3 and 10 wt.% of the fillers at 80 °C and 95% RH. The result is analogous to that reported in other studies [2,3,7,22]. In addition, the performance efficiencies of the PEMFCs equipped with 3 wt.% loading of the TiO_2 fillers are all higher than those with 10 wt.% loading of the corresponding TiO_2 fillers. This implies that the higher loading of the TiO_2 particles did not lead to a higher effect on PEMFC performance as expected, and is ascribed to the possible aggregation of the TiO_2 filler in the composite membranes. This resulted in reduction of the effective surface area as reported in other studies [3,21]. Therefore, the rest of the study

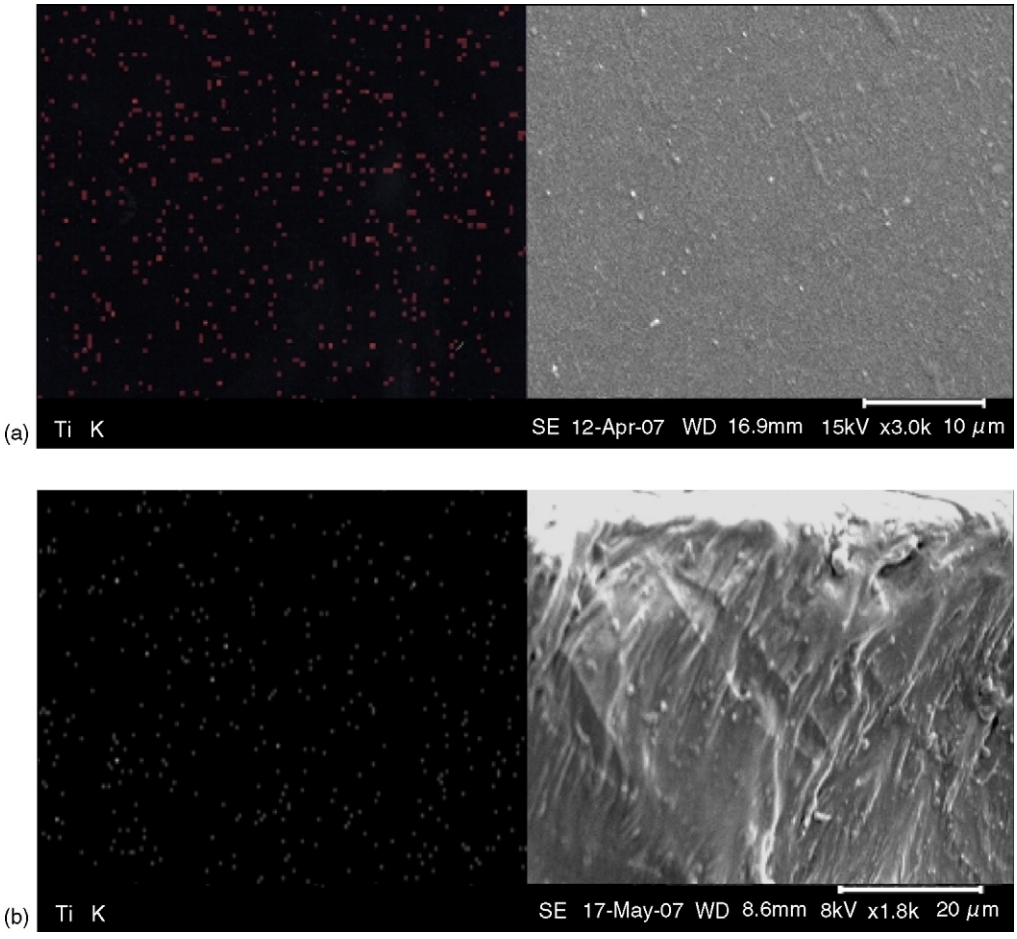

Fig. 7. SEM microphotograph (right) and the corresponding SEM-EDS Ti mapping (left) of NF3P: (a) surface and (b) cross-section.

is only based on the membranes with 3 wt.% loading of the TiO_2 fillers.

As is known, the Nafion-based membranes are generally more humidity sensitive under a reduced RH environment [21,22]. Therefore, the efficiencies of the as-prepared PEMFCs with the as-prepared composite membranes under a reduced RH are also investigated. As found in Fig. 9, at 80 °C when the RH value reduced from 95% to 50%, the current density is reduced to 92.1% of its original value for PEM-NF3P, 91.7% for PEM-NF3C, 93.2% for PEM-NF3B, 94.5% for PEM-NF3N and 81.9% for RNF. It also shows that under the reduced RH, the current densities obtained for PEM-NF3P, PEM-NF3C, PEM-NF3B, and PEM-NF3N are 1.67, 1.33, 1.22, and 1.05 times of PEM-RNF, respectively, indicating a similar decreasing order obtained at 95% RH shown above. The power densities obtained in this condition are 853, 655, 600, 516, and 493 mW cm^{-2} for PEM-NF3P, PEM-NF3C, PEM-NF3B, PEM-NF3N, and PEM-RNF, respectively. The best current density is obtained from PEM-NF3P and is 1.67 times of that obtained from PEM-RNF. The results indicate that the enhancement effects of all the TiO_2 fillers, including P25, on the PEMFCs efficiencies are more pronounced under the low RH (50%) than under the high RH (95%). Although in general, the performance is poorer at a low RH than at a high RH, all the as-prepared Nafion/TiO_2 composite membranes show a higher performance over the recast Nafion membrane under 50% RH at 80 °C, but the one with P25 is lower than all those with the as-prepared TiO_2. This is ascribed to the modification of the membrane with the hygroscopic porous TiO_2 particles, which provides better water retention than that with nonporous TiO_2 and the bare Nafion membrane. Furthermore, the result also demonstrates that although it exhibits the lowest value among the three PEMFCs with the porous anatase-containing composite membranes under the same condition, the performance of the NF3B membrane at 50% RH is comparable to that of RNF at 95% RH, supporting that the enhancement effect of the as-prepared TiO_2 filler on the PEMFC performance is more profound at a low RH.

In addition, the cell tests were carried out at various temperatures (80, 90, 110, and 120 °C) under 50% RH to evaluate the temperature dependence of the as-prepared mesoporous anatase TiO_2 on the cell performance at the low RH. As shown in Fig. 10, under the low RH, the performances of all the as-prepared PEMFCs decreased as the temperature increased. This is ascribed mainly to the increase of the dehydration rate of the membranes by the increase of temperature as shown in Fig. 11. The order of the performances measured at 90 °C is the same as that measured at 80 °C, i.e. PEM-NF3P > PEM-NF3C > PEM-NF3B > PEM-NF3N > PEM-RNF. This order is also consistent with the order of the SSA values of the fillers, revealing that under the reduced RH, the performance of the Nafion-based composite membrane

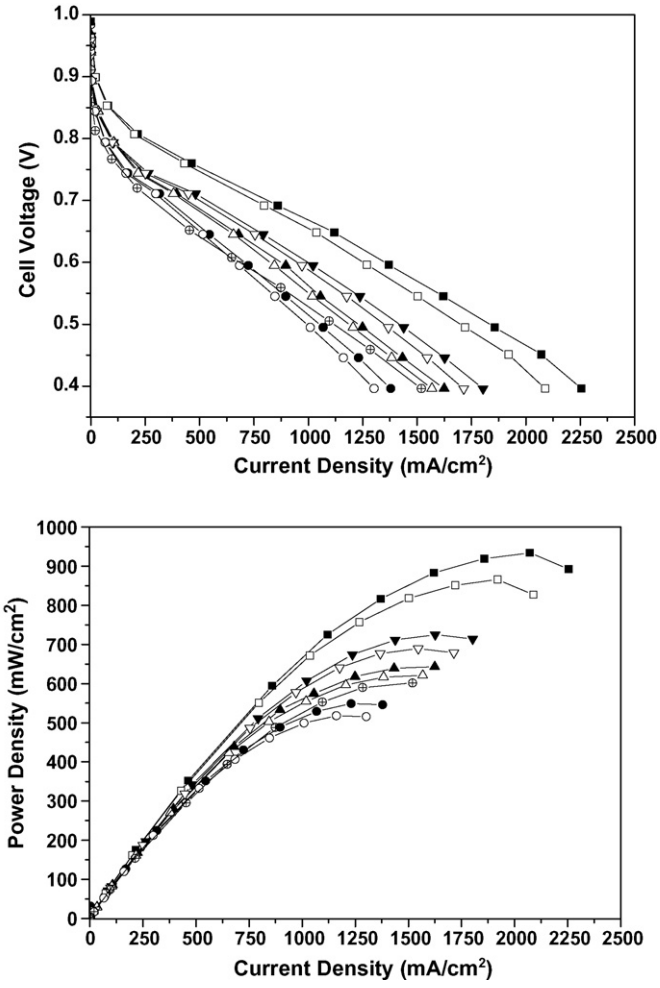

Fig. 8. Performance of the H_2/O_2 PEMFC based on the recast Nafion and the Nafion/TiO_2 composite membranes at 80 °C, 95% RH. (■) PEM-NF3P; (□) PEM-NF10P; (▲) PEM-NF3B; (△) PEM-NF10B; (▼) PEM-NF3C; (▽) PEM-NF10C; (●) PEM-NF3N; (○) PEM-NF10N; (⊕) PEM-RNF.

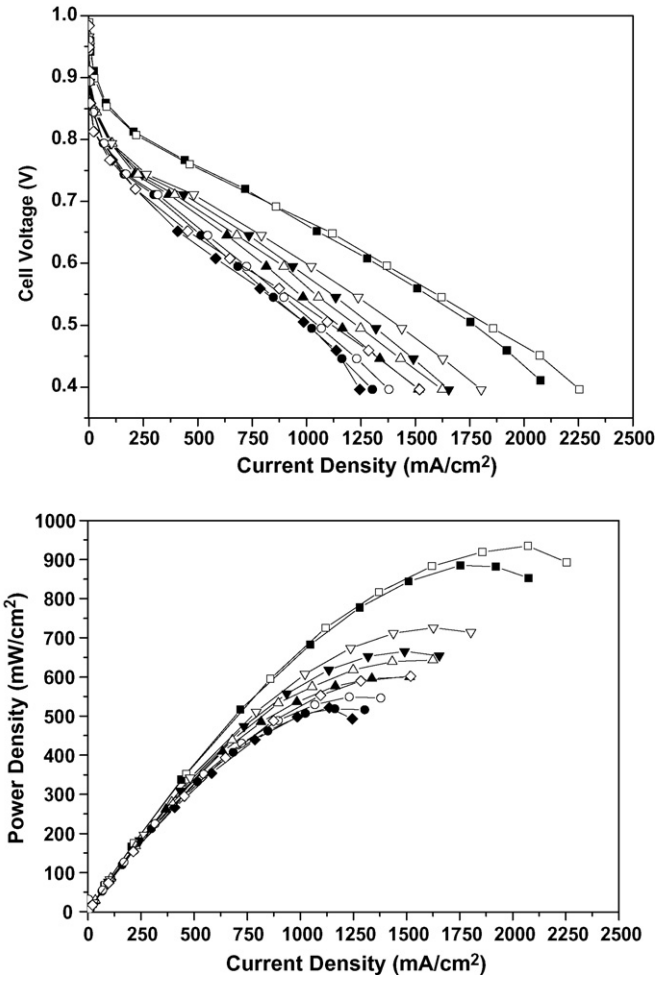

Fig. 9. Performance of the H_2/O_2 PEMFCs at 80 °C, under 50% RH (solid) and 95% RH (hollow). (■, □) PEM-NF3P; (▲, △) PEM-NF3B; (▼, ▽) PEM-NF3C; (●, ○) PEM-NF3N; (♦, ◊) PEM-RNF.

is mainly associated with the SSA value of the filler at this temperature range. However, as summarized in Table 3, when the operating temperature reached 110 and 120 °C, the order of the performances became PEM-NF3P > PEM-NF3B > PEM-NF3C > PEM-NF3N > PEM-RNF. That is, the order between the current densities of PEM-NF3B and PEM-NF3C was reversed. This is attributed to the morphological differences among the TiO_2 fillers, in which P25 refers to nonporous particles containing only the adsorbed water on the particle's surface. Meanwhile,

Table 3
Current density data of the PEMFCs with the Nafion-based membranes at various temperatures and 0.4 V under 50% RH

PEMFC sample	Current density (mA cm^{-2})			
	80 °C	90 °C	110 °C	120 °C
PEM-NF3P	2075	1936	1774	1625
PEM-NF3B	1515	1451	1345	1199
PEM-NF3C	1653	1551	1306	1104
PEM-NF3N	1303	1216	1165	932
PEM-RNF	1245	959	459	285

The pores in $T_{conventional}$ are larger, containing mostly free water that is more easily evaporated, while that in T_{PF6} and T_{BF4} are mesoporous, better confining water molecules in the mesopores. The attribution is confirmed by their dehydration rates (DHR) depicted in Fig. 11. The DHRs of all the membranes increase with an increase in temperature, and the orders of the DHR values at each temperature are consistent with the order of their performance shown above. Particularly, the value for NF3C is lower at 80 °C and about the same at 90 °C, but it becomes higher than that for NF3B as the temperature reaches above 100 °C. The results suggest that not only is the water retention capacity of the filler important for enhancing the performance of the TiO_2-containing Nafion composite membrane in PEMFC operated at a low RH and high temperature, but also the reduction of the dehydration rate caused by the presence of the filler. In this study, the best current density (1625 mA cm^{-2}) obtained under 50% RH at 120 °C and a cell voltage of 0.4 V is from PEM-NF3P and is about 5.7 times higher than that obtained from PEM-RNF (285 mA cm^{-2}). This is ascribed to the optimal morphological properties of T_{PF6}, the highest surface area and the largest amount of homogeneous mesopores, which lead to the best water retention and the least dehydration rate among the

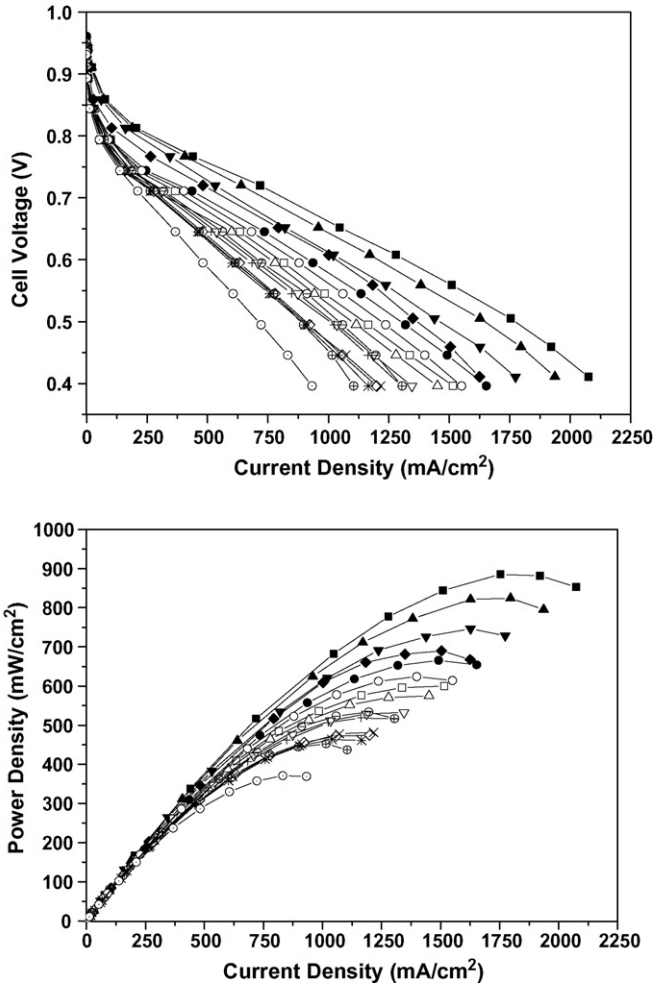

Fig. 10. Performance of the H_2/O_2 PEMFCs at various temperatures and 50% RH. PEM-NF3P: (■) 80 °C, (▲) 90 °C, (▼) 110 °C, (♦) 120 °C; PEM-NF3B: (□) 80 °C, (△) 90 °C, (▽) 110 °C, (◇) 120 °C; PEM-NF3C: (●) 80 °C, (○) 90 °C, (⊖) 110 °C, (⊕) 120 °C; PEM-NF3N: (+) 80 °C, (×) 90 °C, (✳) 110 °C, (⊙) 120 °C.

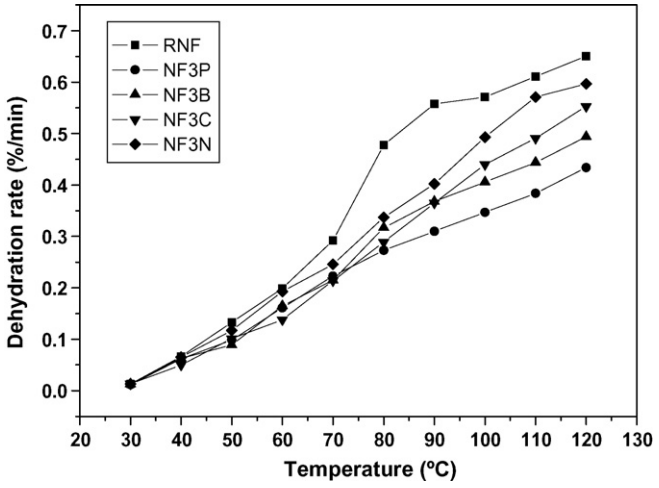

Fig. 11. Dehydration rates of the Nafion-based membranes as a function of temperature at 50% RH.

as-prepared Nafion/TiO_2 composite membranes under the high temperature and the low RH condition applied.

4. Conclusions

In this study, three porous anatase TiO_2 powders were synthesized. T_{PF6} and T_{BF4} were prepared by the modified sol–gel process, using ionic liquids as templates, while $T_{conventional}$ was prepared by the conventional sol–gel method without using ionic liquid as template. Through the morphological characterization, it showed that after calcination at 450 °C, T_{PF6} and T_{BF4} remained mesoporous in structure, while $T_{conventional}$ became mainly microporous. In addition, T_{PF6} had the highest surface area and the largest amount of mesopores with the smallest pore size. These three TiO_2 powders were, then, used as fillers to prepare the composite membranes with Nafion. Among the three composite membranes, the T_{PF6}-containing composite membrane provided the best cell performance in the temperature range of 80–120 °C under 50% and 95% relative humidity. More specifically, when tested in the lower temperatures of 80 and 90 °C at both RH conditions, the surface area of the filler, which reflects its water retention capacity, played a key factor in enhancing cell performance. However, when tested at the higher temperatures of 110 and 120 °C under 50% RH, the size and the amount of mesopores in the filler, which influenced the reduction of the dehydration rate of the Nafion composite, became more important factors than the surface area. As a result, under 50% RH at 120 °C, the best power density (669 mW cm^{-2}) delivered at a voltage of 0.4 V was obtained from the PEMFC with 3 wt.% of T_{PF6} in the composite membrane. It was 5.7 times higher than the value obtained from the recast Nafion membrane.

Acknowledgements

The authors would like to thank National Science Council of ROC (Grant number: NSC 94-2113-M-033-010) and Chung Yuan Christian University of Taiwan, ROC (Grant number: CYCU-95-CR-CH) for financially supporting this research work. The authors are grateful to Dr. Diganta Saikia for helpful discussions.

References

[1] K.A. Mauritz, R.B. Moore, Chem. Rev. 104 (2004) 4535–4585.
[2] V. Baglio, A.S. Aricò, A. Di Blasi, V. Antonucci, P.L. Antonucci, S. Licoccia, E. Traversa, F. Serraino Fiory, Electrochim. Acta 50 (2005) 1241–1246.
[3] V. Baglio, A. Di Blasi, A.S. Aricò, V. Antonucci, P.L. Antonucci, C. Trakanprapai, V. Esposito, S. Licoccia, E. Traversab, J. Electrochem. Soc. 152 (7) (2005) A1373–A1377.
[4] S. Ren, G. Sun, C. Li, S. Song, Q. Xin, X. Yang, J. Power Sources 157 (2006) 724–726.
[5] Z.G. Shao, P. Joghee, I.M. Hsing, J. Membr. Sci. 229 (1–2) (2004) 43–51.
[6] A. Saccà, A. Carbone, E. Passalacqua, A. D'Epifanio, S. Licoccia, E. Traversa, E. Sala, F. Traini, R. Ornelas, J. Power Sources 152 (2005) 16–21.
[7] C. Trakanprapai, V. Esposito, S. Licoccia, E. Traversa, J. Mater. Res. 20 (1) (2005) 128–134.
[8] W. Apichatachuapan, R.B. Moore, K.A. Mauritz, J. Appl. Polym. Sci. 62 (2) (1996) 417–426.

[9] C. Yang, S. Srinivasan, A.S. Aricò, P. Cretı, V. Baglio, V. Antonucci, Electrochem. Solid-State Lett. 4 (4) (2001) A31–A34.
[10] N.H. Jalani, K. Dunn, R. Datta, Electrochim. Acta 51 (3) (2005) 553–560.
[11] F. Bauer, M. Willert-Porada, J. Power Sources 145 (2005) 101–107.
[12] R.V. Gummaraju, R.B. Moore, K.A. Mauritz, J. Polym. Sci. B: Polym. Phys. 34 (14) (1996) 2383–2392.
[13] K.A. Mauritz, Mater. Sci. Eng. C 6 (2–3) (1998) 121–133.
[14] P.L. Antonucci, A.S. Aricò, P. Cretì, E. Ramunni, V. Antonucci, Solid State Ionics 125 (1999) 431–437.
[15] S.K. Young, W.L. Jarrent, K.A. Mauritz, Polymer 43 (2002) 2311–2320.
[16] K.A. Mauritz, D.A. Mountz, D.A. Reuschle, R.I. Blackwell, Electrochim. Acta 50 (2004) 565–569.
[17] K.A. Mauritz, J.T. Payne, J. Membr. Sci. 168 (1–2) (2000) 39–51.
[18] K.T. Adjemian, S.J. Lee, S. Srinivasan, J. Electrochem. Soc. 149 (3) (2002) A256–A261.
[19] D.H. Jung, S.Y. Cho, D.H. Peck, D.R. Shin, J.S. Kim, J. Power Sources 106 (1–2) (2002) 173–177.
[20] H. Nakajima, S. Nomura, T. Sugimoto, S. Nishikawa, I. Honma, J. Electrochem. Soc. 149 (8) (2002) A953–A959.
[21] E. Chalkova, M.B. Pague, M.V. Fedkin, D.J. Wesolowski, S.N. Lvova, J. Electrochem. Soc. 152 (6) (2005) A1035–A1040.
[22] E. Chalkova, M.V. Fedkin, D.J. Wesolowski, S.N. Lvov, J. Electrochem. Soc. 152 (9) (2005) A1742–A1747.
[23] A.S. Aricò, P. Cretì, P.L. Antonucci, V. Antonucci, Electrochem. Solid-State Lett. 1 (2) (1998) 66–68.
[24] B. Libby, W.H. Smyrl, E.L. Cussler, Electrochem. Solid-State Lett. 4 (12) (2001) A197–A199.
[25] A.C. Pierre, G.M. Pajonk, Chem. Rev. 102 (2002) 4243–4265.
[26] S. Dai, Y.H. Ju, H.J. Gao, J.S. Lin, S.J. Pennycook, C.E. Barnes, Chem. Commun. 3 (2000) 243–244.
[27] P. Yang, D. Zhao, D.I. Margolese, B.F. Chemlka, G.D. Stucky, Chem. Mater. 11 (1999) 2813–2826.
[28] D.M. Antonelli, Micropor. Mesopor. Mater. 30 (1999) 315–319.
[29] Z.Y. Peng, Z. Shi, M.L. Liu, Chem. Commun. 21 (2000) 2125–2126.
[30] H. Yoshitake, T. Sugihara, T. Tatsumi, Chem. Mater. 14 (2002) 1023–1029.
[31] K.S. Yoo, T.G. Lee, J. Kim, Micropor. Mesopor. Mater. 84 (2005) 211–217.
[32] P.A.Z. Suarez, J.E.L. Dullius, S.R. Einloft, D.E. Souza, J. Dupont, Polyhedron 15 (7) (1996) 1217–1219.
[33] Y. Zhang, G. Li, Y. Wu, Y. Luo, L. Zhang, J. Phys. Chem. B 109 (12) (2005) 5478–5481.
[34] R.C. Rau, Adv. X-Ray Anal. 6 (1963) 191–201.
[35] D.J. Mead, R.M. Fuoss, J. Am. Chem. Soc. 62 (1940) 1720–1723.
[36] S. Gavalda, K.E. Gubbins, Y. Hanzawa, K. Kaneko, K.T. Thomson, Langmuir 18 (2002) 2141–2151.
[37] K.S.W. Sing, D.H. Everett, R.A.W. Haul, L. Moscou, R.A. Pierotti, J. Rouquerol, T. Siemieniewska, Pure Appl. Chem. 57 (1985) 603–619.